

Battery Cloud with Advanced Algorithms

XIAOJUN LI*
DAVID JAUERNIG
MENGZHU GAO
TREVOR JONES

Gotion Inc
48660 Kato Road, Fremont, California, USA
t.li@gotion.com

Contents

0.1	Introduction	4
0.2	Battery in the Cloud	6
0.2.1	Data Sources and Connections	6
0.2.2	Database	7
0.2.3	Data Visualization	8
0.2.4	Algorithms and Analytics	9
0.3	Onboard SOC Estimation with Cloud-trained ANN	10
0.3.1	Requirements Definition and Design	11
0.3.2	ANN Training with Cloud Data	12
0.3.3	HIL and Vehicle Testing Results	13
0.4	Online State-of-Health Estimation	14
0.4.1	Degradation Mechanisms and Modes of Li-Ion Batteries	15
0.4.2	State-of-Health & End-of-Life	17
0.4.3	Advanced Online SOH-Estimation Methods	19
0.5	Cloud-based Thermal Runaway Prediction	24
0.5.1	Cause and Effects of Thermal Runaway	24
0.5.2	Methods for Thermal Runaway detection	27
0.5.3	Data-driven Thermal Anomaly Detection	28

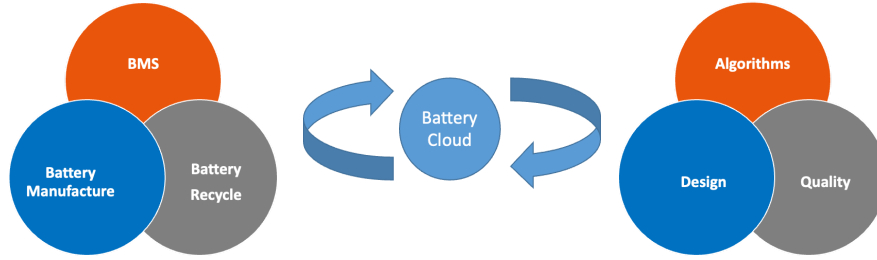


Figure 1: Battery Cloud is at the center of the success of the future battery industry.

0.1 Introduction

Batteries have played an essential role in the rapid development of transportation electrification and energy storage system[1]. Lithium-ion batteries are known for their high energy/power density and low self-discharge. They are becoming more available as the manufacturing cost continues to improve. Large-scale energy storage systems consist of MWh/GWh batteries that continuously operate under different weather conditions. Electric vehicles batteries are subject to road harshness, different driving behavior, and frequent high C-rate fast charges. These applications call for batteries to become more reliable, safe, and predictable. As such, monitoring and control of Li-ion batteries become more critical.

As of now, conventional onboard battery management systems (BMS) are used for monitoring and control. A BMS includes embedded micro-controllers (μC) and peripheral integrated circuitry (IC). Usually, the BMS collects voltage, current, and temperature measurement with dedicated sensing ICs that communicates with a main μC , which process the measurements and perform various functions, such as SOX estimation, diagnostics, protection, control, and thermal management. Nevertheless, the micro-controllers are designed to handle simple tasks and have minimal computing power and memory size. It prevents the onboard BMS from executing advanced algorithms. For example, artificial neural networks (ANN) are frequently used for SOC estimation[2]. As we will

show later in this chapter, an onboard BMS might run a trained neural network. However, the ANN must be carefully designed to reduce CPU and RAM impact. Although the BMS receives numerous data from the measurements of hundreds of cells that it monitors, these data are not stored due to the lack of onboard data storage, making incremental learning impossible for the onboard BMS.

With the further development of IoT[3], future BMS is expected to be cloud-connected (Battery Cloud). As a result, battery data can be seamlessly uploaded and stored in a cloud data platform[4, 5], and the power of cloud computing resources can be leveraged. The cloud computational power and data storage can support advanced algorithms, such as machine learning algorithms improve battery safety, performance, and economy. There are several significant advantages. Firstly, the cloud database has battery data from not just one pack but numerous EV/ESS battery packs, allowing a massive amount of data to be used for extensive data analysis and machine learning. Secondly, cloud computing allows complicated algorithms to be executed in real-time, which is not possible for onboard μ C. Thirdly, the cloud platform allows data collection and feedback from batteries throughout the entire life cycle. This means the other batteries processes and applications also benefit from the battery cloud, such as manufacturing, second life usage, and recycling.

In the remainder of this chapter, at first, critical components of a Battery Cloud are discussed in the first section. Then, in the following sections, we overview the critical areas regarding battery performance, health, and safety: State-of-Charge estimation, State-of-Health estimation, and thermal runaway/anomaly detection. We also present corresponding algorithms that developed with the Battery Cloud. In the first section, we train and validate an artificial neural network (ANN) to estimate pack SOC during vehicle charging using remote vehicle data. The ANN is then implemented and tested by onboard BMS. It gives high accurate ($\approx 3\%$) real-life vehicle testing results. In the second section, high accuracy ($\approx 5\%$) and onboard battery state of health estimation (SOH) methods for electric vehicles are developed based on the differential voltage (DVA) and incremental capacity analysis (ICA). We extract the charging cycles and calcu-

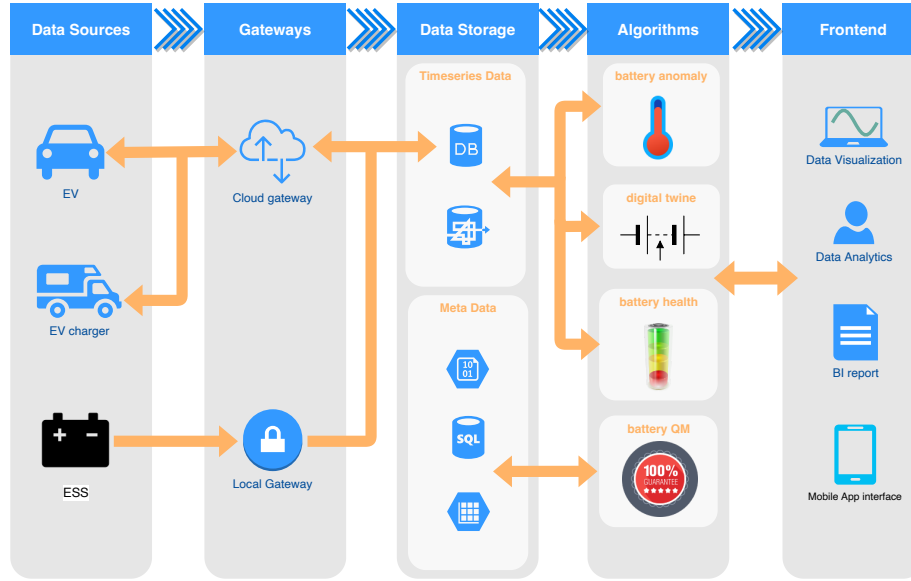


Figure 2: Key hardware and software components and data flow of the Battery Cloud

late the DVA and ICA curves using cloud data. Multiple features are extracted and analyzed to estimate the SOH. In the last section, a data-driven thermal anomaly detection method is developed for battery safety. The method can detect unforeseen thermal anomalies at an early stage, more than 1hr ahead of the event.

0.2 Battery in the Cloud

This section covers essential components for a Battery Cloud, including the database, data visualization, and algorithm/analytics.

0.2.1 Data Sources and Connections

Data are collected during different stages of the battery's life cycle, ranging from cell manufacture and module/pack assembly to vehicle driving/charging and pack recycling. There are numerous procedures for cell manufacture alone,

Table 1: Battery Data Sources

Item	Stages	Type of data
Cell	manufacture	manufacture metadata
	testing	battery timeseries data
Pack	assembly	assembly metadata
	testing	battery timeseries data
EV&ESS	operating	battery timeseries data
		vehicle/grid timeseries data
		vehicle/grid metadata
	service	service record
Charger	operating	charger timeseries data
Pack	recycle	recycle metadata

including electrode mixing, coating, laser cutting, stack, and so many others[6], during which a significant amount of data is generated. Table 1 summarizes battery-related data based on the different devices and scenarios. The EV battery pack is equipped with a BMS, a wireless IoT component that transmits the collected data to the cloud via the 4G/5G network. These data will be collected via the internet, online or private gateways for charging stations. Because ESS power plants affect grid stability, they are subject to more stringent cybersecurity regulations. As a result, usually, ESSs are connected through a one-way, local gateway to ensure maximum security. Similarly, battery data from cell/pack testing equipment are uploaded via a secured, one-way gateway. However, the equipment may be controlled securely via the company’s intranet.

0.2.2 Database

Choosing the right database For production big data platforms, Hadoop[7] is the prevailing choice. Hadoop is based on HDFS (Hadoop files system) and MapReduce (the programming model) that ensure good scalability, robustness, and high availability, all of which are essential requirements for a battery

database. Besides, Hadoop has a complete ecosystem, including software stacks like Spark, Hbase, Kafka, Hive, and many others, making it easier to use and expand functionalities. There are also dedicated timeseries databases (TSDB), such as Influxdb, Timescale, and Prometheus. TSDB has built-in features for timeseries data, such as time-domain queries (integration, differential), retention policy, and others. This makes TSDB ideal for a small R&D battery database. As TSDBs are being developed and improved actively, they will become more competitive against traditional databases in the future.

Database deployment The database can be hosted on primes or on the cloud. Although on-primes deployment will theoretically give better control and security, it is often more expensive to maintain and scale. For cloud deployment, there are several models to consider. IaaS (Infrastructure as a Service) let the cloud provider handle hardware resources, where the company has complete control of software stacks. Popular IaaS providers are Amazon Web Services (AWS)[8], Microsoft Azure[9], and Google Cloud Platform (GCP)[10]. In the PaaS (Data Platform as a Service) model, such as AWS EMR, the cloud provider also hosts basic software stacks, except for application software. The provider manages all software stacks in the SaaS (Software as a Service) model, such as Cloudera[11] and Influxdata Cloud[12].

0.2.3 Data Visualization

Most end-users are data analysts or operators who monitor EV/ESS in real-time. It is vital to have a responsive and interactive data visualization tool where essential data are displayed in real-time. Users can create a dashboard and add custom processing/query to explore statistical insights. Other features include: 1) adding a signal threshold, which can trigger quick alarms to the ESS site operator. 2) Options to trigger an ML pipeline from the frontend. Widespread data visualization tools are web-based, such as Grafana, Datadog, and Kibana. Figure 0.2.3 depicts an example battery data display dashboard.



Figure 3: A typical dashboard for displaying battery data, developed by Gotion[5].

0.2.4 Algorithms and Analytics

With the data platform built, advanced algorithms that leverage big data and machine learning[2] can be applied to increase battery performance, safety and economy. Another interesting topic is the digital twin [13]. Based on sophisticated electrochemical modeling, the digital twin can give insight into the internal states of its physical twin. The battery cloud platform will need API (application programming interface) for popular programming languages, such as Python and Matlab, based on the developers' preferences. It may also provide a more interactive computing platform like the Jupyter notebook/Lab, commonly used for data analytics. After the algorithms/analytics are developed, they should be optimized and incorporated into a data processing engine, such as Spark, Kafka, and Airflow. Life data of all the battery cells are used to analyze the manufacture, assembly process, and facility to improve quality management. Similarly, these data can be used as references during battery second life application, recycling, and refurbishing, eliminating the need for extra testing/calibration.

0.3 Onboard SOC Estimation with Cloud-trained ANN

State of Charge (SOC) estimation is one of the essential functions of battery software. It has been researched extensively. There are mainly three different methods for SOC estimation. The commonly used, basic method is coulomb counting, which calculates the accumulated charge by current integral, given as

$$z(t) = \frac{1}{C} \int i(t)dt + z(0), \quad (1)$$

where C is the battery capacity. This method is susceptible to accumulated error generated from $i(t)$ or data loss from $z(0)$. As such, estimation accuracy degrades if coulomb counting is used without correction over a prolonged period of time. The other two methods are model-based and data-driven. Both have self-correction features to correct SOC. The model-based approach utilizes a battery model, either ECM (equivalent circuit model) or electrochemical model, to establish the connection between battery measurements, such as voltage, temperature, and current, and immeasurable internal states. Then an estimator, such as Kalman Filter, is applied to estimate the SOC. Because those batteries are highly nonlinear systems, modified Kalman filters such as extended Kalman filters and unscented Kalman filters are often used in practice. Model-based approaches require an accurate model. The model can be calibrated accurately by long-term cell and pack testing. But it is also prone to over-fitting, meaning it can not tolerate individual cell/pack variations. Making an accurate and well-generalized model is very challenging and time-consuming. Data-driven approaches range from simple voltage-based correction[14] to deep neural networks[15]. More detailed reviews of data-driven SOC estimation methods are covered by [2, 16]. Most of these methods are resource-consuming and can not be easily applied to an onboard BMS.

This section will present a data-driven SOC estimation method that fuses the onboard BMS with the battery cloud. A neural network is firstly trained with

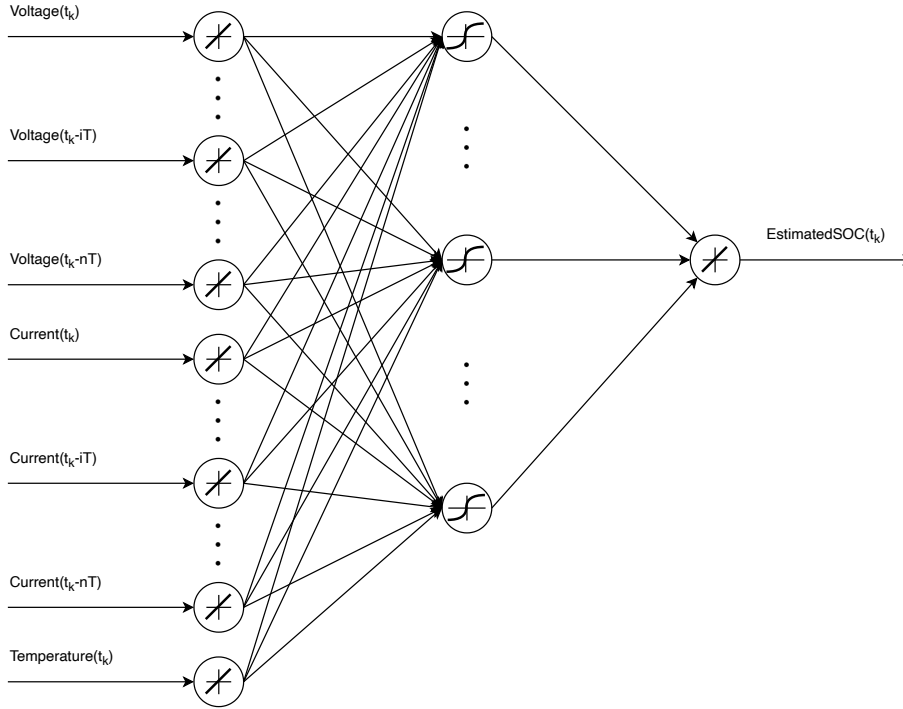


Figure 4: The neural network model used for SOC estimation

cloud battery data. The neural network is designed to reduce its computational and memory footprint to be fit into a micro-controller.

0.3.1 Requirements Definition and Design

When designing SOC algorithms, there are several typical requirements to be considered. For example:

- SOC estimation should be 100% when the battery is fully charged.
- SOC estimation should not change suddenly, including power cycles.
- SOC estimation should have a maximum error of less than 5%.
- SOC estimation should have an average error of less than 3%.

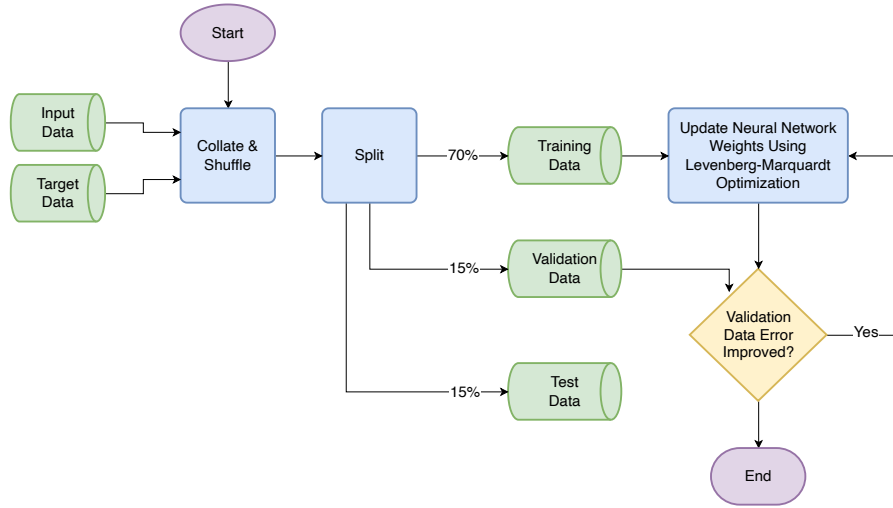


Figure 5: The ANN training flowchart for SOC estimation

The neural network presented is designed to meet requirements #1, #3, and #4. Other requirements, like #2 are implemented by a different software component, such as the SOC initialization function.

As depicted in 4, the neural network includes an input layer, hidden layers, and an output layer. The inputs are measurable battery signals, including voltage, current, and temperature. Both present and historical measurements are used. Historical measurements are critical for the feed-forward ANN to infer the internal SOC of the battery, which is a dynamical system.

0.3.2 ANN Training with Cloud Data

The ANN is developed using Matlab/Simulink. Cloud battery data are fetched through Matlab API and used to train the neural network. DC charging data of LFP cells are used for training. The training data includes the cells being charged at a range of temperatures, including -10° , 0° , 25° , 40° , and 50° , during which the voltage and current signals are recorded. As depicted in Fig 5, these data are split into training data (75%), validation data(15%), and test

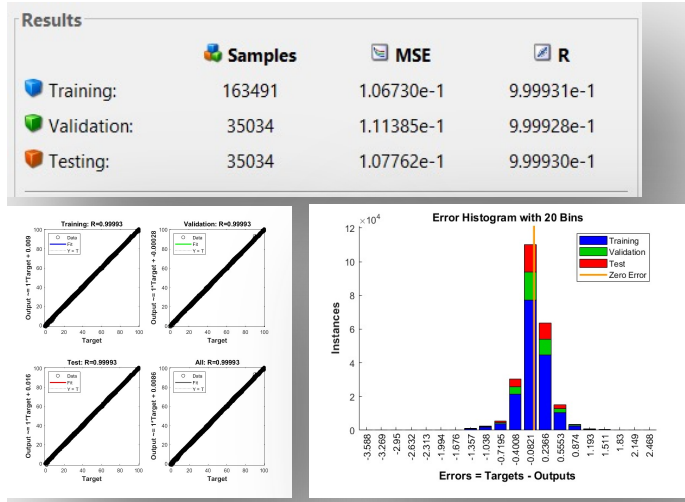


Figure 6: ANN training results

data (15%). During the training, Levenberg-Marquardt is configured as the optimization algorithm. The training results are depicted in Fig 6.

After acquiring the parameters, the ANN is implemented as Matlab code and integrated into the SOC software component, a Simulink model. Using the embedded coder, the Simulink model is converted to C code, integrated with other software components, and eventually become executable binaries.

0.3.3 HIL and Vehicle Testing Results

The ANN is first tested using the hardware-in-the-loop (HIL) system, during which basic functions of the software component and SOC accuracy are evaluated using cloud data. More importantly, as the ANN executes in the BMS real-time operating system (RTOS), the impact on CPU and RAM usage is evaluated. It is found that the ANN takes approximately 50 μ s of execution time. Its RAM usage is also small.

Finally, the algorithm is tested on a vehicle BMS. The ANN is deployed as a shadowing strategy in addition to existing software for several passenger EVs. To verify its robustness, the ANN is tested under the AC charge scenario to

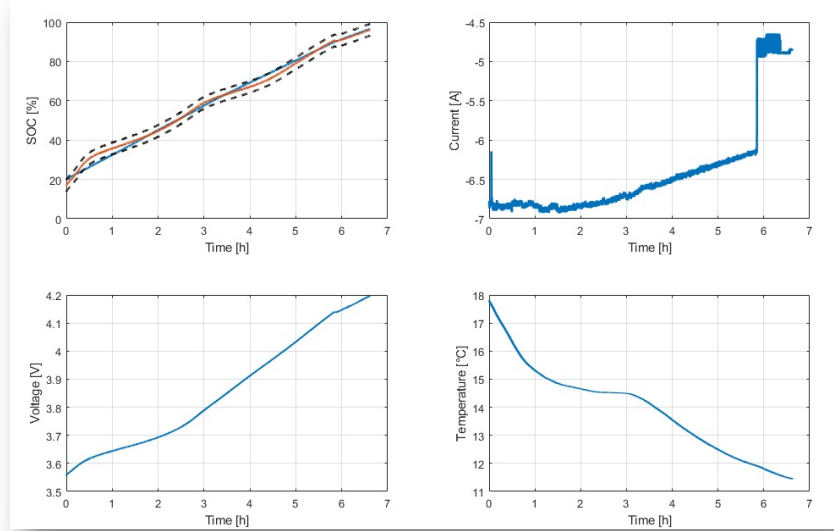


Figure 7: Onboard Vehicle Test: AC charging

verify its robustness. Even though it is only trained with DC charge data, the ANN performed satisfactorily during AC. For example, Fig 7 depicts the SOC comparison, current, voltage, and temperature plots of one test. As shown in the SOC comparison plot, for most of the time, the true SOC (solid blue) falls into the $\pm 5\%$ bracket of the SOC estimation (solid red). The RMSE of all testing results is 1.9%, well below the 3% target.

0.4 Online State-of-Health Estimation

Li-ion batteries and many other secondary cells are subject to different degradation mechanisms that lead to a loss of removable energy or power, which lead to a decrease in range and acceleration for battery electric vehicle [17]. For that reason, it is essential to monitor the state of health of Li-ion batteries. The degradation mechanisms are briefly discussed and organized into three categories in the following section. Furthermore, the concept of the end-of-life

(EOL) and the SOH_C will be presented. Conclusively, an overview of SOH_C estimation methods will be given, with a closer look at the voltage analysis (DVA) and the incremental capacitance analysis (ICA).

0.4.1 Degradation Mechanisms and Modes of Li-Ion Batteries

The components of a Li-ion battery are subject to different degradation mechanisms. In general, the degradation mechanisms can be classified into three modes [17, 18, 19]:

- **Loss of Lithium Inventory (LLI):** Li-ions are consumed by parasitic reactions and are no longer available for cycling between positive and negative electrodes.
- **Loss of active material of the anode (LAM_A):** Active mass of the anode is no longer available for lithium intercalation due to particle cracking and loss of electrical contact or blockage of active sites by resistive surface layers.
- **Loss of active material of the cathode (LAM_C):** Active mass of the cathode is no longer available for the intercalation of lithium due to structural disorder, particle cracking, or loss of electrical contact.

These modes can be attributed to different degradation mechanisms in the components of a Li-ion cell. In the following, the primary degradation mechanisms on the components of a Li-ion cell are named and briefly explained. An overview of these degradation mechanisms is presented in the figure8.

Anode The main degradation modes at the negative electrode are Lithium Plating and the formation of solid electrolyte interphase (SEI). Lithium plating is a commonly recognized and inherently damaging degradation mechanism in Li-ion batteries, which describes the deposition of lithium metal on the surface of the anode as soon as the anode potential exceeds the threshold of 0V

(vs. Li/Li+) [20]. On the other hand, the solid electrolyte interphase (SEI) is a protective layer on the surface of the anode particles due to the decomposition of the electrolyte, which is formed mainly during the first cycles [21]. Both degradation modes are the main contributor for LLI and LAM_A [17].

Cathode On the other side of the battery, the degradation modes of the cathode are still growing in interest and therefore not thoroughly documented yet. It is considered that structural changes and mechanical stress are the main contributors to LLI and LAM_C. Due to various cathode materials, the Li-ion battery suffers from different side reactions based on the cathode material composition. For example, an Mn-based cathode is more prone to the dissolution of the active material due to Mn dissolution. In contrast, the degradation of the LFP cathode is more likely to be defined by Fe dissolution, which generates HF as a by-product and attacks the surface of the cathode particles [20].

Separator, Electrolyte and Current Collectors The separator, the electrolyte, and the current collectors are also subject to various degradation mechanisms. The porous separator of a Li-ion cell, although electrochemically inactive, can significantly affect the performance of the Li-ion cell. Aging studies have shown that deposits from electrolyte decomposition clog the pores of the separator, which leads to an increase in ionic impedance and can also reduce the accessible active surface area of the electrodes (LAM_A and LAM_C, respectively) [18, 22]. On the other hand, the electrolyte is involved in decomposition reactions leading to surface film formation on both electrodes. Since the concentration of the conducting salt determines the ionic conductivity between the two electrodes, the decomposition reactions affect the ohmic resistance of the Li-ion cell. Electrolyte reduction at the anode consumes cyclizable lithium (LLI) and results in a loss of capacity. In contrast, electrolyte oxidation at the cathode does not consume cyclizable lithium but causes re-intercalation into the cathode, corresponding to the cell's self-discharge [23, 24]. There are two main degradation mechanisms for the current collectors of a Li-ion cell. First,

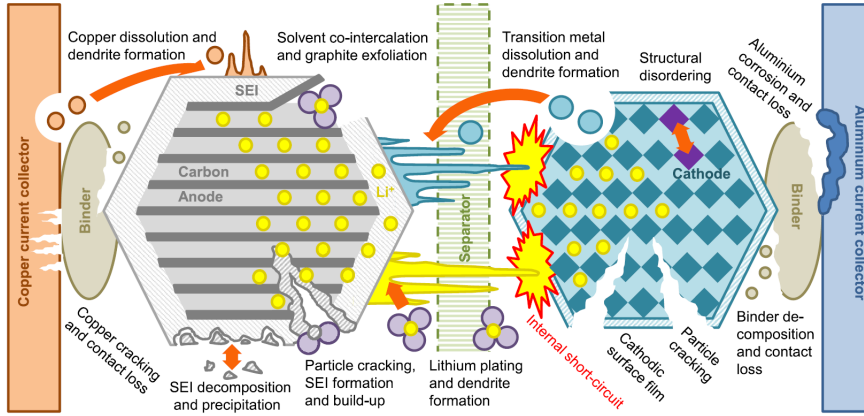


Figure 8: Degradation mechanisms in Li-ion cells [17]

the current collectors can corrode electrochemically. This occurs particularly at the aluminum collector of the positive electrode when acidic species, such as HF, are present and leads to increased contact resistance between the current collector foil and the active material of the cathode [25]. The copper current collector of the negative electrode may dissolve during deep discharge when the anode potential increases to 1.5 V concerning Li/Li⁺ [26]. Second, the current collector foils may deform due to mechanical stress. This can disrupt the contact between the electrodes and the separator so that certain areas can no longer contribute to the cell's capacity [27].

Based on the figure 9, it can be seen that all degradation modes can be organized by their effect on the electric characteristics of a Li-ion battery, the capacity, and power fade. For further elaborations, we will focus primarily on the capacity fade.

0.4.2 State-of-Health & End-of-Life

Due to the degradation mechanisms, Li-ion batteries have a limited lifetime. The end of life (EOL) of a Li-ion battery is reached when the battery can no longer provide the power or energy intended for its application [28]. However,

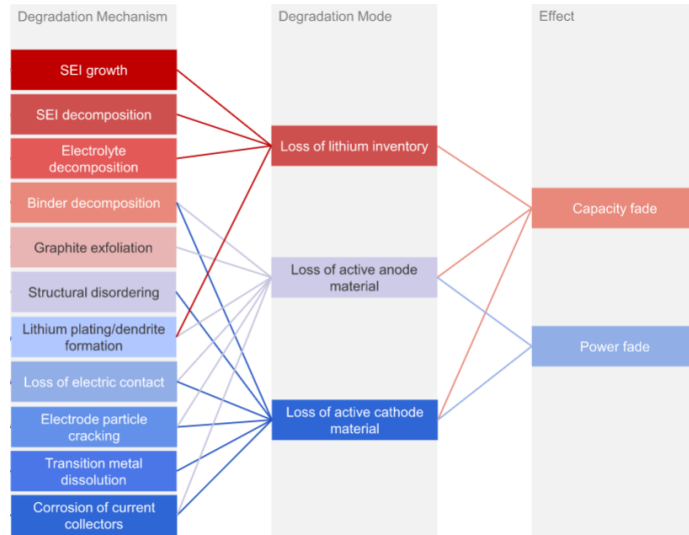


Figure 9: Overview of different degradation mechanisms and their impact adapted from Birkl et al. [17]

as of today, there is no uniform standard that defines a clear EOL criterion for Li-ion batteries in the automotive industry [23]. The USABC consortium is the only one to define two EOL criteria in its manual of test procedures for electric vehicle batteries. According to this manual, the EOL of a Li-ion battery is reached when:

- the net capacity delivered is less than 80% of the rated capacity C_N or,
- the peak capacity is less than 80% of the rated capacity at a DOD of 80% [29].

Also, in many publications, the EOL for the Li-ion-based traction battery of a BEV at a capacitive aging condition of $SOH_C \leq 80\%$ assumed [30, 31, 32]. The capacitive aging state SOH_C can be calculated using equation 2. Here, C_N corresponds to the nominal capacity of the Li-ion battery, and $Q_{dis,max}$ corresponds to the maximum charge quantity that can be removed from a Li-

ion battery, which is also known as the net capacity.

$$SOH_C = \frac{Q_{dis,max}}{C_N} \cdot 100\% \quad (2)$$

0.4.3 Advanced Online SOH-Estimation Methods

The capacitive aging state SOH_C has an impact on two critical factors of a BEV, the maximum range and the charging time during fast charging. Based on the capacitive aging state SOH_C , the maximum range can be predicted to the driver, and the fast charging function can be adjusted to find the optimal compromise between minimum charging time and damage of the anode by lithium plating [33]. Therefore, an online SOH_C estimation is essential for automotive applications.

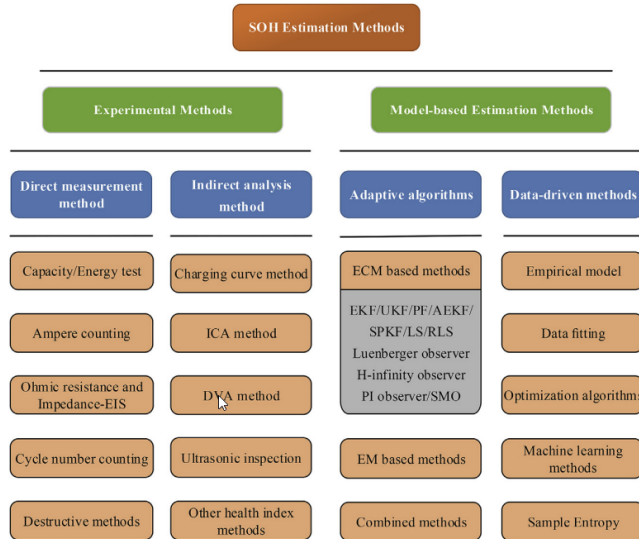


Figure 10: Methods for SOH_C estimation adapted from Xiong et al. [34]

Methods

There are several options for determining the capacitive aging state, which can first be divided into experimental and model-based methods, respectively. As

shown in Fig. 10, these categories can be subdivided into further subcategories. For example, experimental methods can be divided into direct methods, such as capacity measurement (Coulomb counting), and indirect methods, such as differential voltage analysis. In contrast, model-based methods can be divided into SOH_C determination based on adaptive battery models or data-driven methods.

At this point, the most popular methods regarding the capacitive aging condition SOH_C are mentioned and briefly discussed. More detailed summaries about methods for SOH_C estimation were given by Berecibar et al. [35] and Xiong et al. [34].

Direct measurements are the most straightforward method to determine the SOH_C . One prevalent method is the direct measurement of the current battery capacity. However, this method requires an enormous expenditure due to the low charging current during the capacity measurement, which is why this method is only used for R&D purposes.

Model-based estimation methods utilize algorithms like Kalman Filter or Neural Networks to model the battery cell parameters. These methods achieve relatively high accuracy and can be implemented in a Cloud-BMS. Yet, these algorithms require a high development effort. For example, the accuracy of the Kalman filter is highly dependent on the accuracy of the applied battery model, whereby high accuracy is only achieved with complex battery models. Also, training a neural network requires a large amount of data, which can only be generated by cost-intensive testing of battery cells. In addition, these algorithms need extensive validation. For example, the neural network is considered a black box, and the output can not be generally predicted based on unexpected input data.

Indirect analysis methods utilize various battery parameters to correlate the capacity fade with various features of the Li-ion battery. For example, the charge curve can characterize the SOH_C of the battery as it changes throughout

the battery degradation. Constant current followed by constant voltage with current limiting (CCCV) charging mode is commonly used for batteries. Eddahch et al.[36] developed a method for SOH_C estimation using the CV stage as a health indicator. Since minimal intrinsic information about the battery can be obtained directly from the voltage curves, Dubarry et al. [37, 38], for example, used electrochemical characterization and analysis techniques, incremental capacitance analysis (ICA), and differential voltage analysis (dV/dQ) (DVA). These methods are often applied in laboratories since a low current rate is required to record these differential curves. However, due to the increasing energy of the battery packs and the lower power of AC charging, it is also possible to record the differential curves during an AC charging process in a BEV. For this reason, the basics of the DVA and ICA and their correlation with capacity fade will be discussed in more detail below.

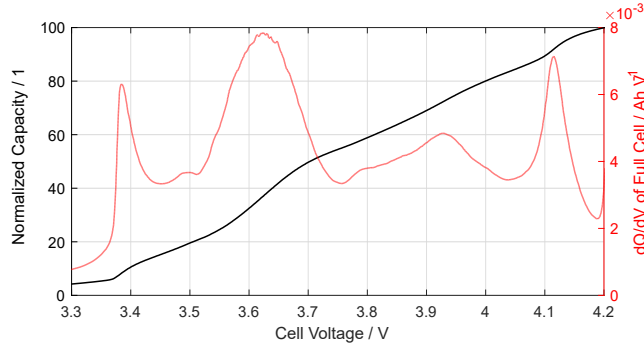


Figure 11: The differential curve of ICA during a CC charge with $C/10$ of a Li-ion battery consisting of a graphite anode and NMC cathode.

DVA/ICA-based SOH-Estimation Method As mentioned before, it is essential to estimate the SOH_C of battery packs in BEV. In the following section, a DVA and ICA-based estimation method is introduced. Therefore, the DVA and ICA will be presented and discussed in detail to present a simple SOH-estimation implementation, which could be realized on a cloud platform.

The DVA and ICA are commonly known analysis methods for Li-ion bat-

teries in laboratories. IC curves can be calculated by integrating the capacity corresponding to small voltage intervals (dQ/dV) by charging or discharging the battery at minimal current rates (see equ. 3). This process converts the voltage plateaus of the two-phase transition into detectable IC peaks. Another method of obtaining more information about aging by processing voltage waveforms is differential voltage analysis (dV/dQ) (DVA). The distance between two peaks of the DV curve represents the amount of current involved in the two-phase transition, so it is easier to analyze capacitance degradation using the DV curves quantitatively [39].

$$\frac{dQ}{dV} \approx \frac{Q(t) - Q(t-1)}{V(t) - V(t-1)} \quad (3)$$

$$\frac{dV}{dQ} = \left(\frac{dQ}{dV}\right)^{-1} \approx \frac{V(t) - V(t-1)}{Q(t) - Q(t-1)} \quad (4)$$

The result of calculating the difference curves during a low current rate charging process is shown in Figure 11. It should be noted that the DV curves can be represented using the half-cell potentials due to the superposition behavior of the anode and cathode (see Eq. 4). Thus, the peaks and valleys of the DV curve can be assigned to the anode and cathode, respectively.

As mentioned before, Li-ion batteries suffer from various degradation mechanisms, which lead to LLI, LAM_C and LAM_A. Due to these degradation modes, a change in the DV and IC curves can be observed. Figure 12 shows the shift of the DV curve due to cyclic aging. In both graphs, the peaks and valleys shift due to structural changes in the electrodes. Based on the change of these features, the SOH_C can be estimated by correlation, for example, the distance between two peaks in the DV curve with the capacity fade of the Li-ion battery. Another possible feature is the height or depth of the peaks or valleys of the IC curve, which also shift throughout the ongoing degradation of battery materials.

DVA/ICA-based SOH estimation on a Battery Cloud includes the following workflow:

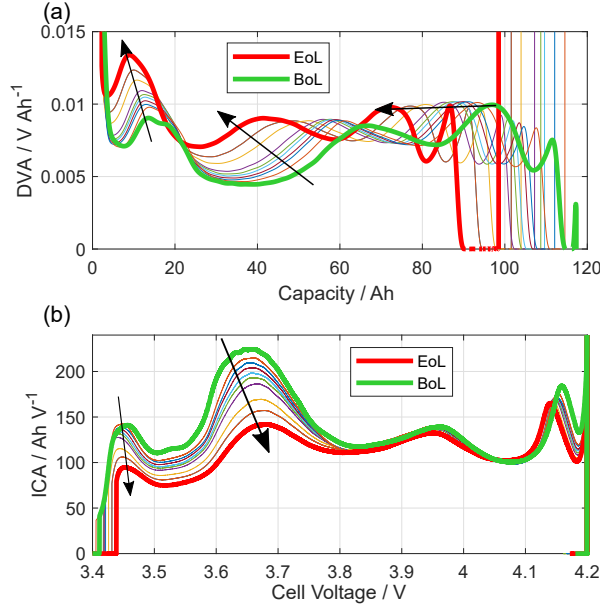


Figure 12: The course of the different curves of the (1) DVA and (2) ICA during a C/3 charge from the beginning of life (BoL) to the end of life (EoL) of a cyclically aged Li-ion battery (graphite anode/NMC cathode).

1. The platform monitors the typical battery cell parameters, voltage, current, and temperature.
2. Whenever the battery is charging, it determines if the charging data has satisfied feature detection based on several conditions. The conditions include the C rates, amount of charge, and so on.
3. If the conditions are met, proceed with the following steps. Otherwise, abort and watch for the next window.
4. Calculate and filter the differential curves (dV/dQ) based on the measurements.
5. Apply feature detection algorithm, i.e., a peak detection algorithm, to extract the features. Based on the scenarios, different features may be

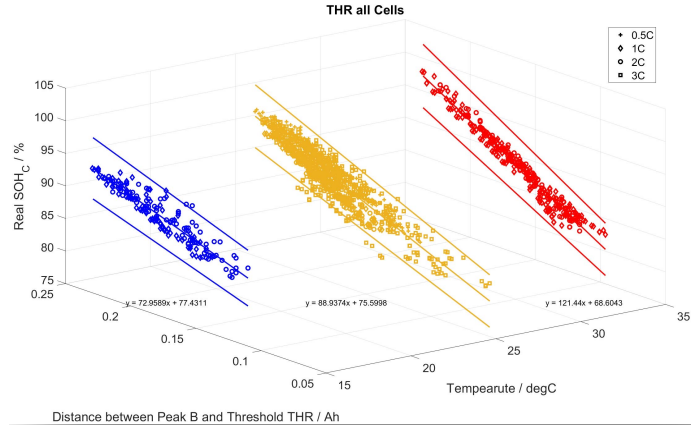


Figure 13: Correlation between DVA/ICA features and real SOH_C , based on various temperatures and C-rates.

extracted and used. Since the features themselves do not indicate the SOH_C , they will be further processed.

6. Apply a mapping function that relates the features with the SOH_C . Typically, the reference is represented by a Look-Up-Table (LUT) that is based on the correlation between features and SOH_C , extracted from existing cyclic aged battery data.

As depicted in Fig 13, the real SOH_C has strong correlations with DVA/ICA features. For example, the distance of peak to peak or peak to valley. The correlations also depend on the temperature. Higher charging currents will affect the estimation accuracy. However, this method can generally achieve 5% SOH accuracy when charging at 3C or less.

0.5 Cloud-based Thermal Runaway Prediction

0.5.1 Cause and Effects of Thermal Runaway

One significant disadvantage of batteries is the narrow operating temperature range. The safety and stability of the battery cells are dependent on keeping

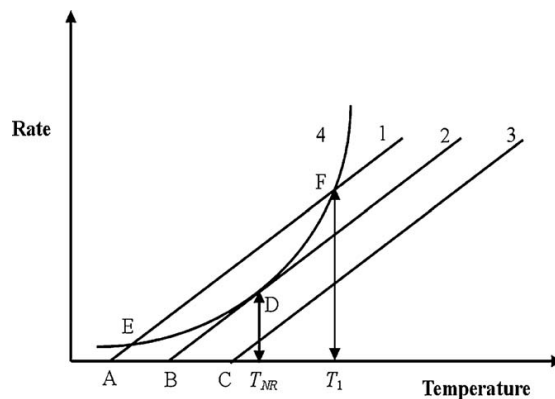


Figure 14: Thermal Runaway explanation based on heat generation and dissipation models[40]

interior temperatures under certain limits. A thermal runaway can occur if the temperature surpasses the critical level, killing the battery or, even worse, causing a fire. Thermal runaway is a chain reaction that can be very difficult to stop once it has begun within a battery cell. During a thermal runaway, the temperature rises incredibly fast (milliseconds), and temperature can be higher than 752°F/400°C. At such elevated temperatures, electrolytes in the battery cell can be vaporized and combustible when exposed to oxygen. Such battery fires are hard to extinguish with conventional ways.

The heat generated by the electrochemical reactions is critical as it can lead to thermal runaway. The heat generation is caused by chemical/electrochemical reactions and joule heating inside the battery. Radiation and convection dissipate heat to the surroundings. The process of thermal runaway can be explained by the plot Fig. 14. The heat generation because of an exothermic reaction assuming Arrhenius law, an exponential function, is shown in curved line 4. In comparison, the heat dissipation is represented by straight lines, which follow Newton's cooling law at different coolant temperatures. For the lithium-ion battery, curve 4 is the combined results of reactions in the cell during the thermal runaway process and the energy balance between the heat generation. Heat

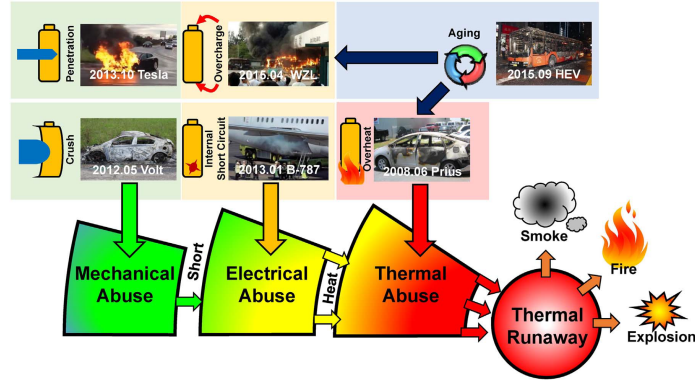


Figure 15: Abuses that cause thermal runaway [41]

dissipation is shown as the following equation Eqn. (5)

$$\frac{\partial(\rho C_p T)}{\partial t} = -\nabla(k\nabla T) + Q_{ab-chem} + Q_{joul} + Q_S + Q_P + Q_{ex} + \dots, \quad (5)$$

where ρ (gcm^{-3}) is the composite/average density of the battery, C_p ($\text{Jg}^{-1} \text{K}^{-1}$) the composite/average heat capacity per unit mass under constant pressure, T (K) the temperature, t (s) the time, k ($\text{Wcm}^{-1}\text{K}^{-1}$) the thermal conductivity. $Q_{ab-chem}$ the abuse chemical reaction in the battery, Q_{joul} Joule heat, Q_s the entropy heat, Q_P the overpotential heat, and Q_{ex} the heat exchange between the system and the ambient.

Generally, thermal runaway can be triggered by various types of abuse in a battery shown in Fig. 15 [41], including:

Internal short circuit Internal short circuit caused by physical damage to the battery or poor battery maintenance.

Mechanical abuse Vehicle collision and consequent crush or penetration of the battery pack are the typical conditions for mechanical abuse.

Electrical abuse

- Overcharging: the voltage that exceeds the maximum safety operation voltage range will damage the battery and lead to thermal runaway. Because of the extra energy filled into the battery during overcharge, the overcharge-induced TR can be more severe than other abuse conditions.
- Rapid charging can lead to excessive currents, therefore, causing thermal runaway
- External short circuit: External short circuit happens when the electrodes with voltage difference are connected by conductors, which could also kick off the TR chain reaction.

Thermal abuse

- Over/Under temperatures: either the low or high side of the safety ranges degrades battery health, leading to irreversible damage that may eventually trigger the TR reaction.
- Contact loose of the cell connector can lead to overheating.

0.5.2 Methods for Thermal Runaway detection

For the typical applications of batteries, including micro-grids and Electric Vehicles, they are connected and packed in modules and packs. Suppose one or a few batteries experience thermal runaway due to the limited space for heat exchange. In that case, the heat will rapidly go up, leading to thermal runaway propagation among all surrounding batteries. Therefore, it's essential to detect thermal runaways at an early stage to ensure operation safety. Lithium-ion batteries may experience a voltage and current anomaly, a temperature rise, or a gas venting during a thermal runaway process. Those are the indicators that can be detected at the early stage of thermal runaway to ensure the operation safety of batteries[42]. Methods of thermal runaway detection include:

Terminal voltage The terminal voltage can be detected by using voltage sensors within the battery management system.

Mechanical deformation Mechanical deformation can be detected by creep distance sensors.

Internal temperature Since the core temperature directly represents the thermal condition within batteries, it can be either:

- measured by temperature sensor inserted in the batteries
- estimated in terms of the measured surface temperature of batteries

Gas component Some gas components can be identified during the thermal runaway process, such as Carbon monoxide, hydrocarbons, and Hydrogen. Gas sensors like thermal conductivity detectors (TCD) can be used for this purpose.

0.5.3 Data-driven Thermal Anomaly Detection

Here we give a cloud-based and data-driven method that monitors the shape-similarities across the measurements to detect battery thermal anomalies[43]. It is robust to battery aging or environment variations since cells are likely to deteriorate or be influenced by these variations as a whole. The shape-based distance measurement handles the asynchronous data issue, which is invariant to signal shifting. Furthermore, this method can be applied to different configurations since it needs very little reference data. This method is based on K-shape clustering[44]

$$SBD(\vec{x}, \vec{y}) = 1 - \max_{\omega} \left(\frac{CC_{\omega}(\mathbf{x}, \mathbf{y})}{\sqrt{R_0(\mathbf{x}, \mathbf{x}) R_0(\mathbf{y}, \mathbf{y})}} \right), \quad (6)$$

where \vec{x}, \vec{y} are the normalized time-series measurements, and R_0 the Rayleigh Quotient. This algorithm has two steps per iteration, repeated until convergence or max iteration is reached.

Workflow

As depicted in Fig. 16, the proposed anomaly detection method contains the following steps. At first, data is continuously buffered and segmented. During

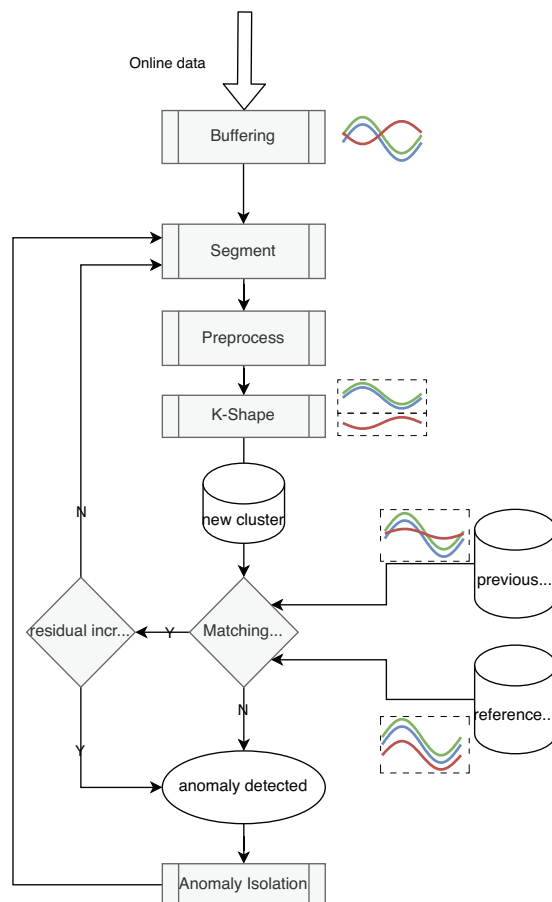


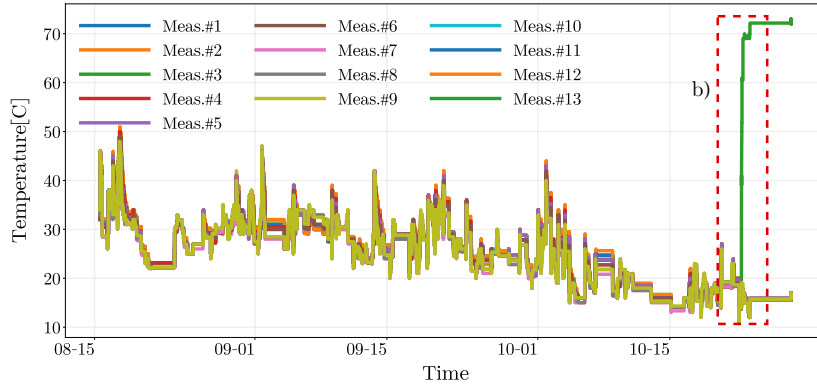
Figure 16: Flowchart

the preprocessing stage, invalid/faulted data points are removed. Signals are normalized. Segments with static signals are filtered out. During the Anomaly Confirmation stage, the K-shape algorithm is applied to each segment for the distances $(SBD(x_i, c_j))$ for each cluster. Two criteria are used for determining anomaly. 1) If one or multiple measurements change its membership, it indicates an anomaly. 2) When no change was found in cluster membership, we check for a significant increase in fitting errors. During each iteration, the i th cluster is compared to the reference cluster for capturing the accumulated changes associated with anomalies that developed gradually. For example, a

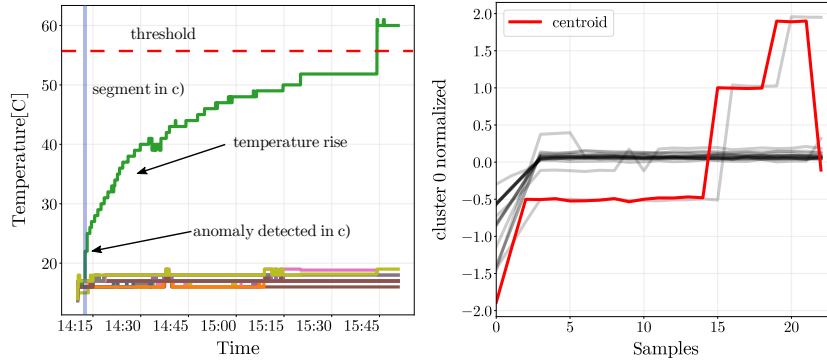
thermal anomaly is caused by the battery's increased internal resistances. It's also compared to the predecessor for anomalies that developed abruptly, such as short-circuit. In the final stage of Anomaly Isolation, we use the change of membership or increase in fitting error to isolate the signals that have caused the anomaly.

Case Study

We apply the proposed anomaly detection method to an EV battery. The data was collected and transmitted from an onboard BMS. As depicted in Fig 17(a), on Oct 30th, the temperature near sensor #13 increased to over 70 °C. The onboard BMS detects the over-temperature anomaly around 3:45 pm, when the maximum temperature is over 55 °C. The proposed method detects anomalies around 2:15 pm, which is about 90 minutes earlier. The timing difference between the two methods is illustrated in Fig 17(b). As it shows, the proposed method detect the anomaly when sensor #13 just started to behave differently from the other measurements. Fig 17(c) shows a shape plot of the segment when the anomaly is detected. In this figure, #13 is flagged as the outlier for its rising shape.



(a) two months of temperature signals, over-temperature highlighted



(b) anomaly detected 90min ahead

(c) one of the signal has different shape

Figure 17: Test Case (a) temperature measurement data with the over-temperature fault. (b) The zoom-in view of fault, this method detects the temperature anomaly 90min before it surpasses the threshold. (c) Further zoom-in view of the segment's shapes plot where the anomaly is detected, which is also highlighted with blue in (b)

Bibliography

- [1] B. Dunn, H. Kamath, J.-m. Tarascon, Electrical energy storage for the Grid : A Battery of choices, *Science Magazine* 334 (6058) (2011) 928–936. doi:10.1126/science.1212741.
- [2] T. Lombardo, M. Duquesnoy, H. El-Bouysidy, F. Áren, A. Gallo-Bueno, P. B. Jørgensen, A. Bhowmik, A. Demortière, E. Ayerbe, F. Alcaide, M. Reynaud, J. Carrasco, A. Grimaud, C. Zhang, T. Vegge, P. Johansson, A. A. Franco, Artificial Intelligence Applied to Battery Research: Hype or Reality?, *Chemical Reviews* doi:10.1021/acs.chemrev.1c00108.
- [3] L. D. Xu, W. He, S. Li, Internet of things in industries: A survey (2014). doi:10.1109/TII.2014.2300753.
- [4] Voltaiq.
URL <https://www.voltaiq.com/>
- [5] How Gotion Monitors its EV Battery Solution with InfluxDB, Grafana and AWS.
URL <https://www.influxdata.com/resources/how-gotion-monitors-its-ev-battery-solution-with-influxdb-grafana-and-aws/>
- [6] J. Schnell, C. Nentwich, F. Endres, A. Kollenda, F. Distel, T. Knoche, G. Reinhart, Data mining in lithium-ion battery cell production, *Journal of Power Sources* 413 (October 2018) (2019) 360–366. doi:10.1016/j.

- jpowsour.2018.12.062.
URL <https://doi.org/10.1016/j.jpowsour.2018.12.062>
- [7] Apache Hadoop.
URL <https://hadoop.apache.org/>
- [8] Amazon Web Service.
URL <https://aws.amazon.com/>
- [9] Microsoft Azure.
URL <https://azure.microsoft.com/>
- [10] Google Cloud Platform.
URL <https://cloud.google.com/>
- [11] Cloudera.
URL <https://www.cloudera.com/>
- [12] influxdata.
URL <https://www.influxdata.com/>
- [13] W. Li, M. Rentemeister, J. Badeda, D. Jöst, D. Schulte, D. U. Sauer, Digital twin for battery systems: Cloud battery management system with online state-of-charge and state-of-health estimation, *Journal of Energy Storage* 30 (April) (2020) 101557. doi:10.1016/j.est.2020.101557.
URL <https://doi.org/10.1016/j.est.2020.101557>
- [14] A. Abdollahi, J. Li, X. Li, T. Jones, A. Habeebullah, Voltage-Based State of Charge Correction at Charge-End, in: *2021 IEEE Vehicle Power and Propulsion Conference (VPPC)*, 2021, pp. 1–6. doi:10.1109/VPPC53923.2021.9699170.
- [15] E. Chemali, P. J. Kollmeyer, M. Preindl, A. Emadi, State-of-charge estimation of Li-ion batteries using deep neural networks: A machine learning approach, *Journal of Power Sources* 400 (June) (2018) 242–255. doi:

- 10.1016/j.jpowsour.2018.06.104.
URL <https://doi.org/10.1016/j.jpowsour.2018.06.104>
- [16] M. A. Hannan, M. S. Lipu, A. Hussain, A. Mohamed, A review of lithium-ion battery state of charge estimation and management system in electric vehicle applications: Challenges and recommendations, *Renewable and Sustainable Energy Reviews* 78 (August 2016) (2017) 834–854. doi:10.1016/j.rser.2017.05.001.
URL <http://dx.doi.org/10.1016/j.rser.2017.05.001>
- [17] C. R. Birkl, M. R. Roberts, E. McTurk, P. G. Bruce, D. A. Howey, Degradation diagnostics for lithium ion cells, *Journal of Power Sources* 341 (2017) 373–386. doi:10.1016/j.jpowsour.2016.12.011.
- [18] J. Vetter, P. Novák, M. R. Wagner, C. Veit, K. C. Möller, J. O. Besenhard, M. Winter, M. Wohlfahrt-Mehrens, C. Vogler, A. Hammouche, Ageing mechanisms in lithium-ion batteries, *Journal of Power Sources* 147 (1-2) (2005) 269–281. doi:10.1016/j.jpowsour.2005.01.006.
- [19] M. Dubarry, C. Truchot, B. Y. Liaw, Synthesize battery degradation modes via a diagnostic and prognostic model, *Journal of Power Sources* 219 (2012) 204–216. doi:10.1016/j.jpowsour.2012.07.016.
- [20] M. M. Kabir, D. E. Demirocak, Degradation mechanisms in Li-ion batteries: a state-of-the-art review (2017). doi:10.1002/er.3762.
- [21] P. Verma, P. Maire, P. Novák, A review of the features and analyses of the solid electrolyte interphase in Li-ion batteries, *Electrochimica Acta* 55 (22) (2010) 6332–6341. doi:10.1016/j.electacta.2010.05.072.
URL <http://www.sciencedirect.com/science/article/pii/S0013468610007747>
- [22] D. Aurbach, B. Markovsky, I. Weissman, E. Levi, Y. Ein-Eli, On the correlation between surface chemistry and performance of graphite negative electrodes for Li ion batteries, *Electrochimica Acta* 45 (1) (1999) 67–86.

- doi:10.1016/S0013-4686(99)00194-2.
URL <http://www.sciencedirect.com/science/article/pii/S0013468699001942>
- [23] P. Keil, A. Jossen, Aging of lithium-ion batteries in electric vehicles: Impact of regenerative braking (2015). doi:10.3390/wevj7010041.
URL <https://mediatum.ub.tum.de/node?id=1355829>
- [24] M. Broussely, P. Biensan, F. Bonhomme, P. Blanchard, S. Herreyre, K. Nechev, R. J. Staniewicz, Main aging mechanisms in Li ion batteries, *Journal of Power Sources* 146 (1-2) (2005) 90–96. doi:10.1016/j.jpowsour.2005.03.172.
URL <http://www.sciencedirect.com/science/article/pii/S0378775305005082>
- [25] P. Arora, R. E. White, M. Doyle, Capacity Fade Mechanisms and Side Reactions in Lithium-Ion Batteries, *Journal of The Electrochemical Society* 145 (10) (1998) 3647–3667. doi:10.1149/1.1838857.
URL <https://iopscience.iop.org/article/10.1149/1.1838857>
- [26] X. Han, L. Lu, Y. Zheng, X. Feng, Z. Li, J. Li, M. Ouyang, A review on the key issues of the lithium ion battery degradation among the whole life cycle, *eTransportation* 1 (2019) 100005. doi:10.1016/j.etrans.2019.100005.
- [27] T. Waldmann, S. Gorse, T. Samtleben, G. Schneider, V. Knoblauch, M. Wohlfahrt-Mehrens, A Mechanical Aging Mechanism in Lithium-Ion Batteries, *Journal of The Electrochemical Society* 161 (10) (2014) A1742–A1747. doi:10.1149/2.1001410jes.
URL <https://iopscience.iop.org/article/10.1149/2.1001410jes>
- [28] R. Korthauer, *Handbuch Lithium-Ionen-Batterien*, Springer Berlin Heidelberg, 2013. doi:10.1007/978-3-642-30653-2.

- [29] USABC, Electric Vehicle Battery Test Procedures - Rev. 2 (1996).
URL http://www.uscar.org/commands/files_download.php?files_id=73
- [30] E. Wood, M. Alexander, T. H. Bradley, Investigation of battery end-of-life conditions for plug-in hybrid electric vehicles, *Journal of Power Sources* 196 (11) (2011) 5147–5154. doi:10.1016/j.jpowsour.2011.02.025.
URL <http://www.sciencedirect.com/science/article/pii/S037877531100379X>
- [31] V. Marano, S. Onori, Y. Guezennec, G. Rizzoni, N. Madella, Lithium-ion batteries life estimation for plug-in hybrid electric vehicles, in: 5th IEEE Vehicle Power and Propulsion Conference, VPPC '09, 2009, pp. 536–543. doi:10.1109/VPPC.2009.5289803.
- [32] Y. Zhang, C. Y. Wang, X. Tang, Cycling degradation of an automotive LiFePO₄ lithium-ion battery, *Journal of Power Sources* 196 (3) (2011) 1513–1520. doi:10.1016/j.jpowsour.2010.08.070.
URL <https://pennstate.pure.elsevier.com/en/publications/cycling-degradation-of-an-automotive-lifeposub4sub-lithium-ion-ba>
- [33] A. Tomaszewska, Z. Chu, X. Feng, S. O’Kane, X. Liu, J. Chen, C. Ji, E. Endler, R. Li, L. Liu, Y. Li, S. Zheng, S. Vetterlein, M. Gao, J. Du, M. Parkes, M. Ouyang, M. Marinescu, G. Offer, B. Wu, Lithium-ion battery fast charging: A review, *eTransportation* 1 (2019) 100011. doi:10.1016/j.etrans.2019.100011.
- [34] R. Xiong, L. Li, J. Tian, Towards a smarter battery management system: A critical review on battery state of health monitoring methods, *Journal of Power Sources* 405 (2018) 18–29. doi:10.1016/j.jpowsour.2018.10.019.
- [35] M. Bercibar, I. Gandiaga, I. Villarreal, N. Omar, J. Van Mierlo, P. Van Den Bossche, Critical review of state of health estimation methods of Li-ion batteries for real applications, *Renewable and Sustainable Energy Reviews* 56 (2016) 572–587. doi:10.1016/j.rser.2015.11.042.

- [36] A. Eddahech, O. Briat, J. M. Vinassa, Determination of lithium-ion battery state-of-health based on constant-voltage charge phase, *Journal of Power Sources* 258. doi:10.1016/j.jpowsour.2014.02.020.
- [37] M. Dubarry, B. Y. Liaw, Identify capacity fading mechanism in a commercial LiFePO₄ cell, *Journal of Power Sources* 194 (1) (2009) 541–549. doi:10.1016/j.jpowsour.2009.05.036.
- [38] M. Dubarry, B. Y. Liaw, M. S. Chen, S. S. Chyan, K. C. Han, W. T. Sie, S. H. Wu, Identifying battery aging mechanisms in large format Li ion cells, *Journal of Power Sources* 196 (7) (2011) 3420–3425. doi:10.1016/j.jpowsour.2010.07.029.
- [39] X. Han, M. Ouyang, L. Lu, J. Li, A comparative study of commercial lithium ion battery cycle life in electric vehicle: Capacity loss estimation, *Journal of Power Sources* 268 (2014) 658–669. doi:10.1016/j.jpowsour.2014.06.111.
URL <http://www.sciencedirect.com/science/article/pii/S0378775314009756>
- [40] Q. Wang, P. Ping, X. Zhao, G. Chu, J. Sun, C. Chen, Thermal runaway caused fire and explosion of lithium ion battery, *Journal of Power Sources* 208 (2012) 210–224. doi:10.1016/j.jpowsour.2012.02.038.
- [41] X. Feng, M. Ouyang, X. Liu, L. Lu, Y. Xia, X. He, Thermal runaway mechanism of lithium ion battery for electric vehicles: A review, *Energy Storage Materials* 10 (2018) 246–267. doi:10.1016/J.ENSM.2017.05.013.
- [42] Z. Liao, S. Zhang, K. Li, G. Zhang, T. G. Habetler, A survey of methods for monitoring and detecting thermal runaway of lithium-ion batteries, *Journal of Power Sources* 436 (2019) 226879. doi:10.1016/J.JPOWSOUR.2019.226879.

- [43] X. Li, J. Li, A. Abdollahi, T. Jones, A. Habeebullah, Data-driven Thermal Anomaly Detection for Batteries using Unsupervised Shape Clustering, Tech. rep. (2021). doi:10.1109/ISIE45552.2021.9576348.
- [44] J. Paparrizos, L. Gravano, K-shape: Efficient and accurate clustering of time series, in: Proceedings of the ACM SIGMOD International Conference on Management of Data, Vol. 2015-May, Association for Computing Machinery, 2015, pp. 1855–1870. doi:10.1145/2723372.2737793.